Nonisothermal Melt Crystallization Kinetics of Syndiotactic Polypropylene/Alumina Nanocomposites

Le Thuy Truong,[1,2] Åge Larsen,[1] Børge Holme,[1] Jaan Roots[2]

[1]*SINTEF Materials and Chemistry, NO-0314 Oslo, Norway*
[2]*Department of Chemistry, University of Oslo, NO-0315 Oslo, Norway*

Received 4 May 2011; accepted 23 January 2012
DOI 10.1002/app.36875
Published online in Wiley Online Library (wileyonlinelibrary.com).

ABSTRACT: Nonisothermal melt crystallization kinetics of syndiotactic polypropylene (sPP)/alumina nanocomposites were investigated via differential scanning calorimetry. The addition of alumina nanoparticles significantly increases the number of nuclei and promotes the crystallization rate of sPP. Nonisothermal melt crystallization kinetics was analyzed by fitting the experimental data to a Nakamura model using Matlab. The average values of Avrami exponent n are 1.7 for both sPP and sPP/Al_2O_3 nanocomposites during slow cooling, which implies a two-dimensional growth is the predominant mechanism of crystallization following a heterogeneous nucleation. The two nanocomposites give n values equal to 2.3 during faster cooling, indicating that the main growth type taking place for sPP/alumina nanocomposites is also the two-dimensional growth. The subsequent melting behavior shows that the presence of alumina nanoparticles changed both the cold crystallization and the recrystallization of sPP. © 2012 Wiley Periodicals, Inc. J Appl Polym Sci 000: 000–000, 2012

Key words: polypropylene (PP); syndiotactic; crystallization; nanoparticles; nucleation

INTRODUCTION

The properties of semi-crystalline polymer such as syndiotactic polypropylene (sPP) are mainly dependent on the structure of the polymer. The structure of the semi-crystalline polymer is controlled by the mechanism of nucleation and crystallization kinetics.[1] The crystallization mechanism is influenced by crystallization temperature, cooling rate, and nucleating agents. The crystallization behavior of sPP has been studied for industrial applications over recent years owing to its interesting properties, such as high flexibility and electrical breakdown strength, and good mechanical ductility.[2–5] Therefore, there have been many studies on crystallization kinetics and crystallinity of sPP over recent years.[6–10]

Besides its excellent elastic properties, the slow crystallization rate is a main disadvantage for the processing behavior, limiting commercial application of this polymer.[5,11] Nanocomposites consisting of sPP and inorganic fillers have attracted much interest of researchers during the last decade to broaden commercial applications of sPP.[12,13] Inorganic fillers have played an important role in the polymer industries. The main purpose of their use is not only for reducing processing time, but also for improving physical and mechanical properties. Inorganic nanoparticles are interesting as a new class of inorganic fillers owing to the high specific surface area. The addition of nanoparticles can enhance the crystallization rates by providing more sites for nucleation and reducing the processing time.[14] Both organic layered silicates and silver nanoparticles significantly increased the crystallization rate of sPP owing to their heterogeneous nucleation effect.[15,16] Alumina nanoparticles were reported as very effective nucleating agents and improved tensile and impact properties of isotactic polypropylene.[17]

Industrial processes usually give nonisothermal crystallization conditions. It is necessary to have quantitative evaluations of nonisothermal crystallization processes for the optimum conditions in industrial applications to achieve the desired properties. Although many investigations have been done on the crystallization kinetics of sPP, studies on the crystallization kinetics of sPP/alumina nanocomposites are very limited. In the present contribution, the nonisothermal melt crystallization of sPP filled with pure Al_2O_3 or hydrophobically coated Al_2O_3 nanoparticles was investigated mainly by differential scanning calorimetry and polarized optical microscopy with a hot stage. The kinetics of the nonisothermal melt crystallization process was analyzed based on a Nakamura model using Matlab.

Correspondence to: Å. Larsen (age.larsen@sintef.no).
Contract grant sponsors: The Research Council of Norway, SINTEF Materials and Chemistry.

CRYSTALLIZATION MODEL

Isothermal crystallization of semi-crystalline polymers has been extensively reported in the scientific literature.[18] The degree of phase transformation, $X(t)$, is related to time by the Avrami equation

$$X(t) = 1 - \exp(kt^n) \quad (1)$$

where $X(t)$ is the crystalline volume fraction, n is the Avrami exponent, and k is the kinetic constant containing nucleation and growth rate. Both constants are characteristics of the crystallization.

Nonisothermal crystallization has been approached by the classical Avrami model and obtaining differential expressions with a temperature-dependent kinetic constant. Nakamura et al.[19–21] introduced the following integral expression obtained from the general Avrami theory

$$X(t) = 1 - \exp\left[-\left(\int K(T)\,dt\right)^n\right] \quad (2)$$

where $K(T)$ is related to the Avrami constant through the relation $K(T) = k(T)^{1/n}$ where T is the absolute temperature.

A differential expression based on the Kolmogorov–Avrami–Evans statistical theory[22,23] and the isokinetic condition introduced by Nakamura et al.,[19–21]

$$\frac{dX}{dt} = nK(T)X_\infty\left(1 - \frac{X}{X_\infty}\right)\left(-\ln\left(1 - \frac{X}{X_\infty}\right)\right)^{(n-1)/n} \quad (3)$$

where X_∞ is the maximum crystallinity volume, n is the Avrami index, and $K(T)$ is a rate function to which we apply a "multimode" version of the traditional Gaussian-shaped rate equation expressed as

$$K(T) = \sum_i K_{\max,i}\exp\left(-4\ln 2 \quad \left(\frac{T - T_{\max,i}}{D_i}\right)^2\right) \quad (4)$$

where D_i, $T_{\max,I}$, and $K_{\max,i}$ are the half width, temperature of maximum and maximum value of the $K(T)$ curve, respectively. The choice of the multimode model was motivated by both DSC crystallization experiments and hot-stage crystallization of samples of varying volume. Equations (2)–(4) were solved by using an explicit time-integration with time-step control and second-order spatial interpolation using Matlab.[24,25] The best-fitting values of the parameters were used for the description of the crystallization kinetics of sPP and sPP/alumina nanocomposites.

EXPERIMENTAL

Materials

sPP manufactured by Total Fina was used as supplied; the commercial sPP had the following characteristics: a melt flow index of 4 g/10 min (230°C/2.16 kg), density 0.88 g/cm^3, and a melting point of 130°C. Spherical γ-phase alumina (Al_2O_3) nanoparticles with nominal size 50 nm were purchased from Sigma-Aldrich (St. Louis, MO, US). (3-Chloropropyl)-triethoxysilane (95%) and anhydrous toluene (99.8 %) obtained from Aldrich were also used as supplied.

Sample preparation

The surface of the alumina was functionalized by silylation reactions to create hydrocarbon groups for improved hydrophobic interaction with a sPP matrix as described in our previous article.[26] The sPP and alumina (pure or surface-modified alumina) were manually premixed, and the mixture was melt blended in a corotating twin-screw batch extruder (DSM Midi 2000) at 70 rpm and 200°C for 5 min. All the nanocomposites contained an equal amount of 3 wt % alumina. The extruded materials were then moulded in a hot press at 200°C and cooled to obtain 1-mm thick films.

Characterization

Nonisothermal crystallization of these resins was investigated by a PerkinElmer Pyris 8500 differential scanning calorimeter (DSC). Calibration for the temperature and heat flow was carried out using standards of indium (T_m = 156.6°C and ΔH = 28.5 J/g) and zinc (T_m = 419.47°C and ΔH = 108.37 J/g). Standard aluminum pans (PerkinElmer 0219-0041) were used to minimize thermal lag between the polymer sample and the DSC furnace. Typical sample sizes were 2–4 mg. All measurements were carried out under nitrogen atmosphere. The crystallization experiment started with heating each sample from 20 to 220°C at a heating rate of 40 K/min and holding at 220°C for 5 min to set a similar thermal history to all samples. The sample was crystallized at various cooling rates. The cooling rates were 1, 10, 25, and 100 K/min. In a separate series of experiments, melting thermograms were recorded at a heating rate of 10 K/min for neat sPP and the 3 wt % pure Al_2O_3/sPP nanocomposite after nonisothermal melt crystallization at cooling rates of 100 and 25 K/min.

A polarizing optical nicroscope (POM) (Olympus BX51, Japan) equipped with a hot stage (Linkam THMS 600) was used to observe the morphology of the neat sPP and the composites. The thin sample pieces ca. 10 μm thick cut from the hot-pressed

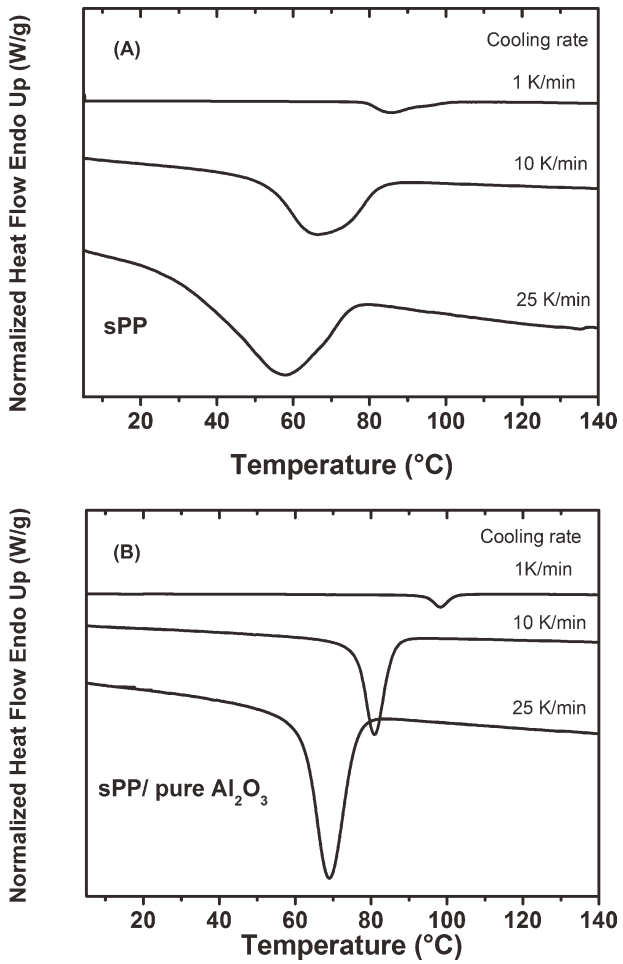

Figure 1 Nonisothermal melt crystallization exotherm of (A) sPP and (B) sPP/pure alumina nanocomposites at various cooling rates.

plates were sandwiched between optical glass plates. Each sample was heated from 20 to 220°C at a rate of 40 K/min, kept at this temperature for 5 min to allow complete melting, and then cooled to room temperature either at 1 or at 10 K/min. Liquid nitrogen was purged through the hot stage for temperature control. The number of crystals was measured with the "ImageJ" software.[27] First, POM images were split into three separate color channels (red, green, and blue) by using split channels. The green channel was selected for subtracting the background. A standard "Gaussian filter" routine was then used to reduce the noise from the POM images. The same value of "Threshold" was applied for all measurements. A bright spot is counted as a nucleus.

RESULTS AND DISCUSSION

Figure 1 shows nonisothermal melt crystallization exotherms of (A) sPP and (B) sPP/pure alumina nanocomposites at various cooling rates. The exothermic peak shifts to a lower temperature and becomes broader as the cooling rate increases for both the neat sPP and the sPP/alumina nanocomposites. At lower cooling rates, there is more time to overcome the nucleation barrier during cooling, and hence crystallization starts at higher temperatures. For the rapidly cooled samples, the activation of nuclei occurs at lower temperatures as expected.

Figure 2 shows nonisothermal melt crystallization exotherms of pristine sPP, sPP/pure alumina, and sPP/modified alumina nanocomposites at various

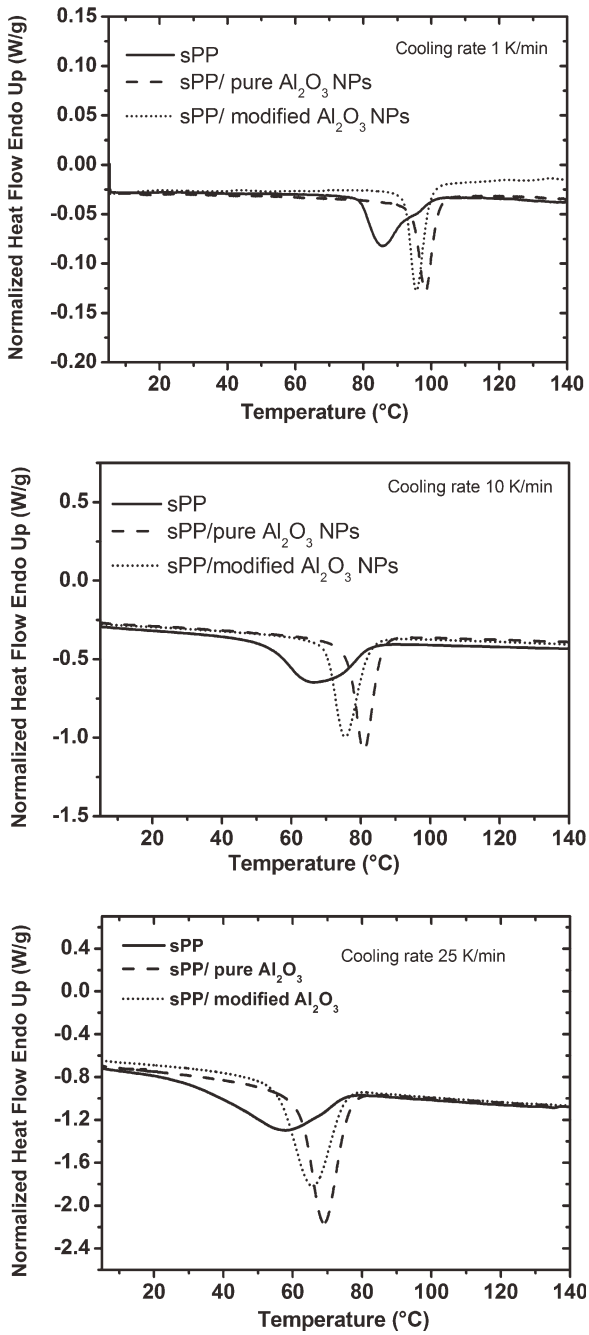

Figure 2 Comparison between neat sPP, sPP/pure Al_2O_3, and sPP/modified-Al_2O_3 nanocomposites for nonisothermal melt crystallization exotherms at various cooling rates.

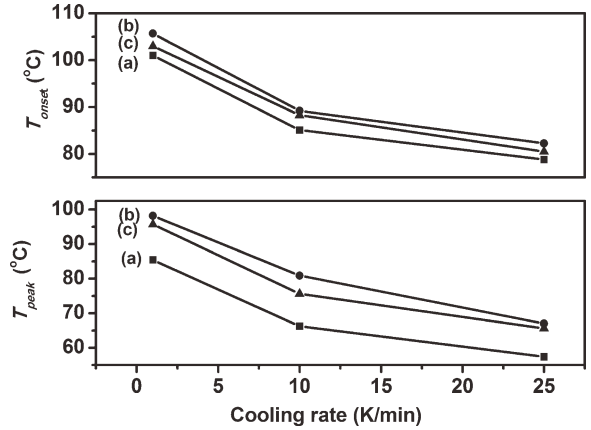

Figure 3 Crystallization peak and onset temperature of neat sPP (a), sPP/pure Al_2O_3 (b), and sPP/modified Al_2O_3 (c) nanocomposites for nonisothermal melt crystallization exotherms as a function of cooling rate.

cooling rates. Figure 2 shows that sPP is a slowly crystallizing polymer. The incorporation of pure alumina increased both peak temperature and onset temperature of crystallization, (here referred to as T_{peak} and T_{onset}, respectively). Comparing the parameters of the pristine sPP to those of pure Al_2O_3/sPP nanocomposites, T_{onset} and T_{peak} at a cooling rate of 1 K/min are increased from 102.2 to 105.7°C and from 85.4 to 98.2°C, respectively. Similarly, at a cooling rate of 10 K/min, T_{onset} and T_{peak} are increased from 85.1 to 89.2°C and from 66.2 to 80.9°C, respectively. The same trend can be seen for a cooling rate of 25 K/min (Fig. 2, bottom, and Fig. 3).

From DSC thermogram shown in Figure 2, the relative crystallinity $X_t(T)$ as a function of temperature can be calculated by integrating the heat flow as given in eq. (5):

$$X_t(T) = \frac{\int_{T_0}^{T} (dH_c/dT) \times dT}{\int_{T_0}^{T_\infty} (dH_c/dT) \times dT} \tag{5}$$

where T_0 and T correspond to the crystallization onset and experimental temperatures, respectively; dH_c/dT represents the variation of the enthalpy of crystallization as a function of temperature variation; and ΔH_c, the overall crystallization enthalpy under a specific cooling rate.

Figure 4 shows the variation of the relative crystallinity X_t as a function of temperature during cooling for pristine sPP, sPP/pure alumina, and sPP/modified alumina nanocomposites at different cooling rates. For all cooling rates, the slope of the $X_t = f(T)$ curves is increased in the presence of alumina nanoparticles and growth starts earlier.

In general, cf. Figures 1, 2, and 4, the incorporation of Al_2O_3 nanoparticles induces heterogeneous nucleation, and thus the crystallization takes place at higher temperatures. The crystallization peak becomes sharper, indicating that the nanoparticles influence the nucleation and result in a faster crystallization. The effect is more noticeable for the composites containing the pure alumina nanoparticles than for the hydrophobically modified one, indicating a more favorable surface structure in pure Al_2O_3 nanoparticles than in modified alumina particles to nucleate the sPP crystals.

The difference in crystallization rates between the two kinds of composites can be attributed to a difference in surface energy and size of the particles. The nucleation rate not only depends on the surface

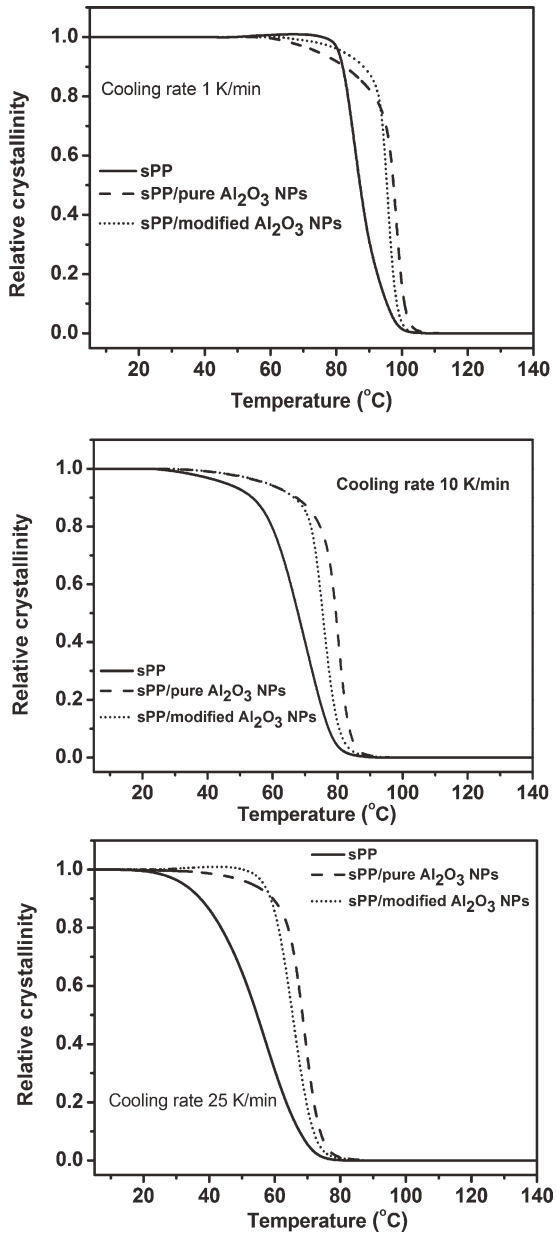

Figure 4 Relative crystallinity as a function of temperature.

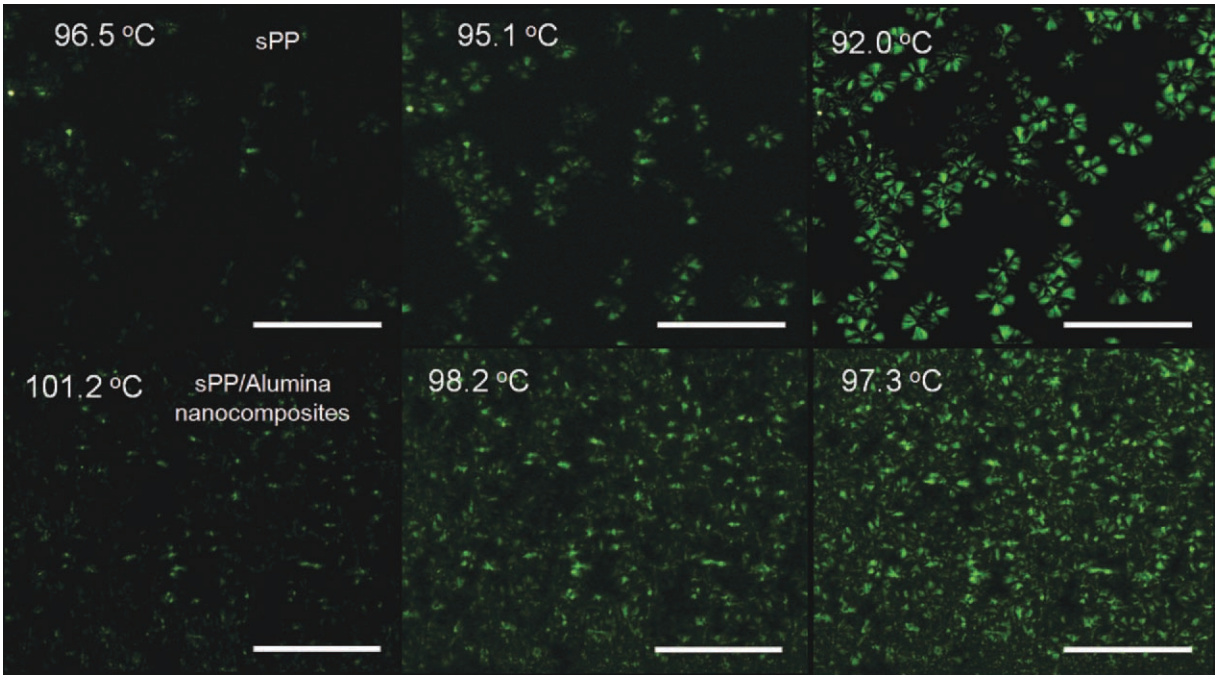

Figure 5 Development of s-PP hedrites of neat sPP (top) and sPP/pure alumina nanocomposites (bottom) at 1 K/min. The scale bar represents 100 μm for all images. [Color figure can be viewed in the online issue, which is available at wileyonlinelibrary.com.]

energy of fillers but also is affected by the geometry of the nucleation surfaces. From a thermodynamics point of view, the presence of a high-energy inorganic surface promotes heterogeneous nucleation of polymers. The higher surface energy of pure alumina nanoparticles gives more effective nucleation sites. Further, the free energy barrier for heterogeneous nucleation for a convex spherical substrate decreases as the substrate radius increases.[28] The aggregation of unmodified particles in the sPP matrix generating larger particles[26] also promotes heterogeneous nucleation.

For a quantitative analysis of nucleation density, the crystallization was carried out using a hot stage connected with a polarized optical microscope (POM). In a study on morphology, we have observed that sPP samples form hedrites by using small-angle light scattering (SALS).[29] Figure 5 shows the examples of the online snapshots, illustrating the development of hedrites at a cooling rate of 1 K/min. The hedrites are randomly distributed over the area of observation. Their density rapidly increases with time. The density of nuclei was calculated from the evolution in the number of hedrites as a function of temperature by using "ImageJ" software.[27] A quantitative study for the nuclei density provides information to understand the effect of processing and composition on physical properties. The results obtained for the density of nuclei are shown in Figure 6(A,B) for 10 and 1 K/min, respectively. As expected, the presence of alumina nanoparticles

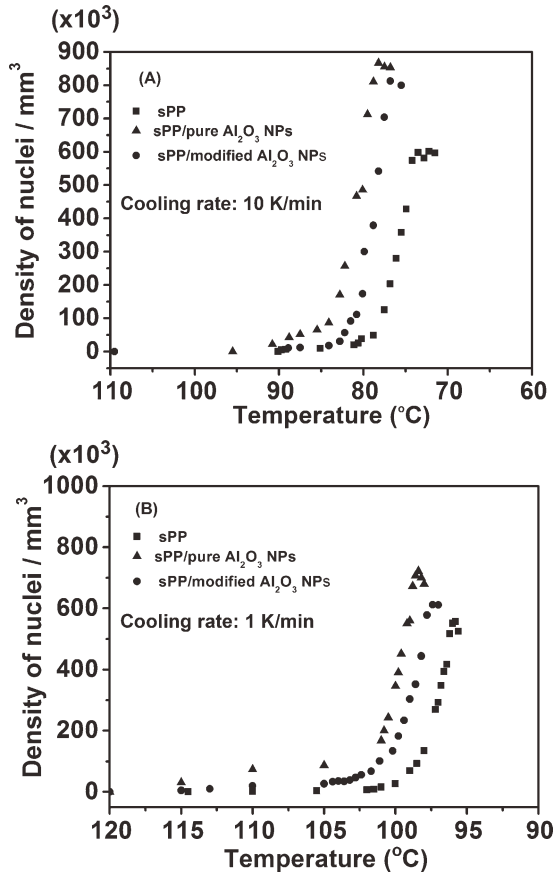

Figure 6 Density of hedrite nuclei as a function of temperature. Determination by microscopic observations during crystallization at 10 K/min (A) and 1 K/min (B).

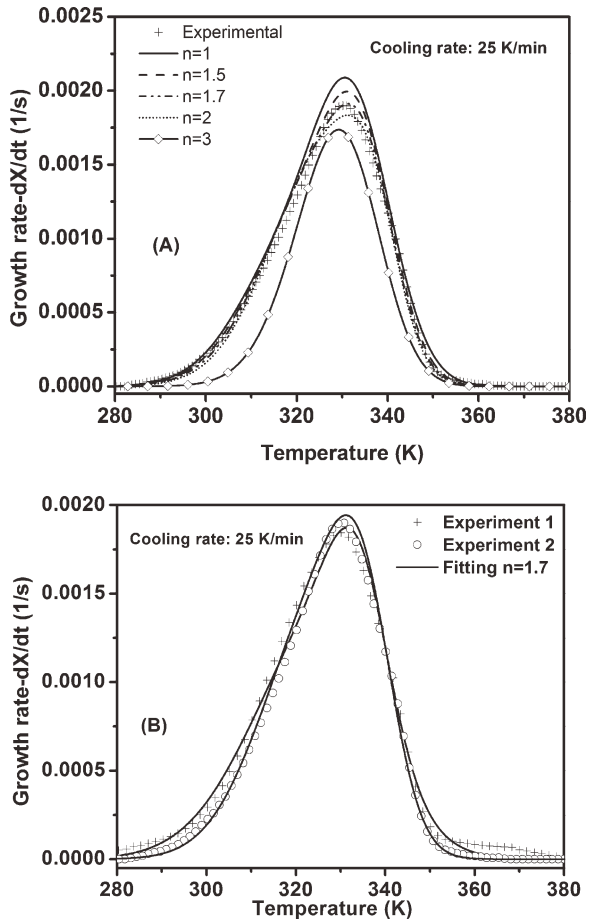

Figure 7 A comparison of the experimental data and the fitting at various Avrami values (A), a comparison between experimental data and the fitting of two parallel experiments (B) for sPP at 25 K/min.

induces heterogeneous nucleation sites, and thus crystallization occurs at a higher temperature, as was seen in the DSC results above.

To predict the kinetics of the crystal structure formation, the growth rates of crystals during nonisothermal crystallization were calculated based on the expressions given above (eqs. (2)–(4)). The model parameters were fitted to experimental DSC data. Figure 7(A) shows a comparison of the experimental data and the fitting at different Avrami values for sPP at 25 K/min. It can be seen that the best-fitting value of the Avrami index is 1.7. Parallel DSC experiments for each sample were carried out to confirm if the results are reproducible [Fig. 7(B)]. Based on these results, we estimated the uncertainty in the Avrami n to be ± 0.1. Similarly, the other curves for all samples were fitted with various n-values ranging from 1 to 3. The best-fitting parameters are listed in Table I. The onset of nonisothermal crystallization is well predicted by the model. This means that the nucleation process is well represented by this approach. The model shows a good agreement with experimental data at various crystallization conditions. As we assumed that crystallization kinetics were controlled by two different crystallization modes, and that the Avrami exponent values are the same for both modes, the model does not fit well with the low temperature shoulder of the crystallization of sPP at 10 K/min (Fig. 8). At the slow cooling rate, 1 K/min, the profile of the growth rate, dX/dt, exhibits a main peak and a shoulder at higher temperature, indicating that the neat sPP from the supplier contains additives which can act as heterogeneous nuclei. To investigate this point, we carried out experiments with crystallization of samples of various thicknesses (data not shown). Reducing the sample thickness to 3 μm, nucleation changed and occurred slower and at lower temperature during cooling. In this case, the sample did not contain the extra nucleation sites because the amount of additives in the sample is not sufficiently high. Multimode is necessary as this mode well reflects a shoulder from DSC data for sPP. At higher cooling rates, 10 and 25 K/min, there is not enough time for the additives to activate, and thus the heterogeneous and homogeneous nucleation may take place simultaneously. The growth rate peaks are quite sharp and steep at the beginning of the phase transition for sPP/alumina nanocomposites (Fig. 9). This shows the presence of a large number of active

TABLE I
Nonisothermal Crystallization Kinetics of sPP and sPP/Alumina Nanocomposites Based on the Nakamura Model

Samples	sPP			sPP/Pure alumina			sPP/Modified alumina		
Cooling rate (K/min)	1	10	25	1	10	25	1	10	25
Avrami index	1.7	1.7	1.7	1.7	1.8	2.3	1.7	1.8	2.3
$K_{max1} \times 10^3 (s^{-1})$	0.4	1.0	2.6	0.8	6.3	11.8	0.8	4.9	9.9
T_{max1} (K)	86.1	75.9	65.2	98.9	82.0	70.5	96.4	76.9	67.9
D_{max1} (K)	5.2	4.5	11.3	3.1	3.8	5.5	3.1	4.6	7.3
$K_{max2} \times 10^3 (s^{-1})$	0.3	2.4	2.5	0.1	0.9	1.5	0.1	1.2	1.5
T_{max2} (K)	95.5	70.4	54.2	94.5	81.3	85.7	87.5	80.0	79.5
D_{max2} (K)	5.7	12.9	18.8	21.6	14.2	36.1	38.9	11.8	21.9

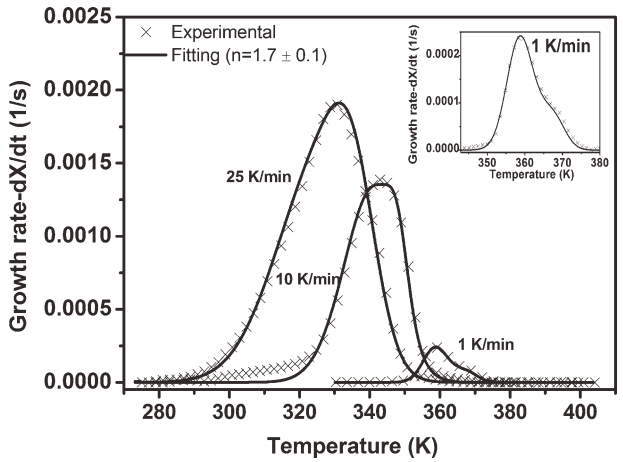

Figure 8 Growth rate of sPP for experimental data (cross) and fitting (solid lines) of the Nakamura model at various cooling rates.

nuclei as shown in Figure 6. Then, at temperatures lower than the peak position, these exotherms become smoother with a low-temperature shoulder.

The best-fitting values of the Avrami index—summarized in Table I—are smaller than those usually reported for syndiotatic polypropylene in isothermal as well as nonisothermal experiments using the classical Avrami equation in both cases.[7,8,30] By using the Nakamura model in the present study, a value of n equals to 1.7 ± 0.1 indicates that a disk-like growth is the predominant mechanism of crystallization. The two sPP/alumina nanocomposites give n-values equal to 2.3 ± 0.1 at faster cooling (25 K/min). This indicates that according to the Nakamura model, the main growth type taking place for these nanocomposites is disk-like. The change in n may relate to a change from two-dimensional growth into a spherulitic-like growth or sporadic nucleation. Our previous SALS results showed no evident spherulite formation under equal cooling conditions.[29] The K_{max} values representing the relative importance of Modes 1 and 2 are significant for sPP which shows a shoulder at slow cooling. This once again justifies the choice of the two-mode model to study. However, for the other samples, Mode 2 is not significant. The width, D_{max}, of the kinetics decreases with the presence of alumina nanoparticles, which relates to faster crystallization. The D_{max} values are also found to increase with faster cooling. T_{max} shifts to lower values with increasing cooling rate because initial crystallization depends on nucleation which takes time. The trends are consistent for Mode 1 of all systems and for Mode 2 of sPP.

To study the dependence between the crystallization conditions, Al_2O_3 nanoparticles incorporation, and the process of cold crystallization, nonisothermal melt crystallizations at two high cooling rates, 100 K/min (A) and 25 K/min (B), were carried out. The thermograms from the subsequent heating at 10 and 150 K/min are shown in Figure 10 for sPP and sPP/pure alumina nanocomposites. Most of the cold crystallization takes place between 20 and 60°C. There are two melting endotherms of the sPP at higher temperature. The lower temperature peak is attributed to the primary crystallites formed at corresponding crystallization conditions and cold crystallization. The higher temperature peak corresponds to the crystal perfection and recrystallization during a subsequent heating scan.[31] At higher heating rate, 150 K/min, the higher T_m peak is reduced because

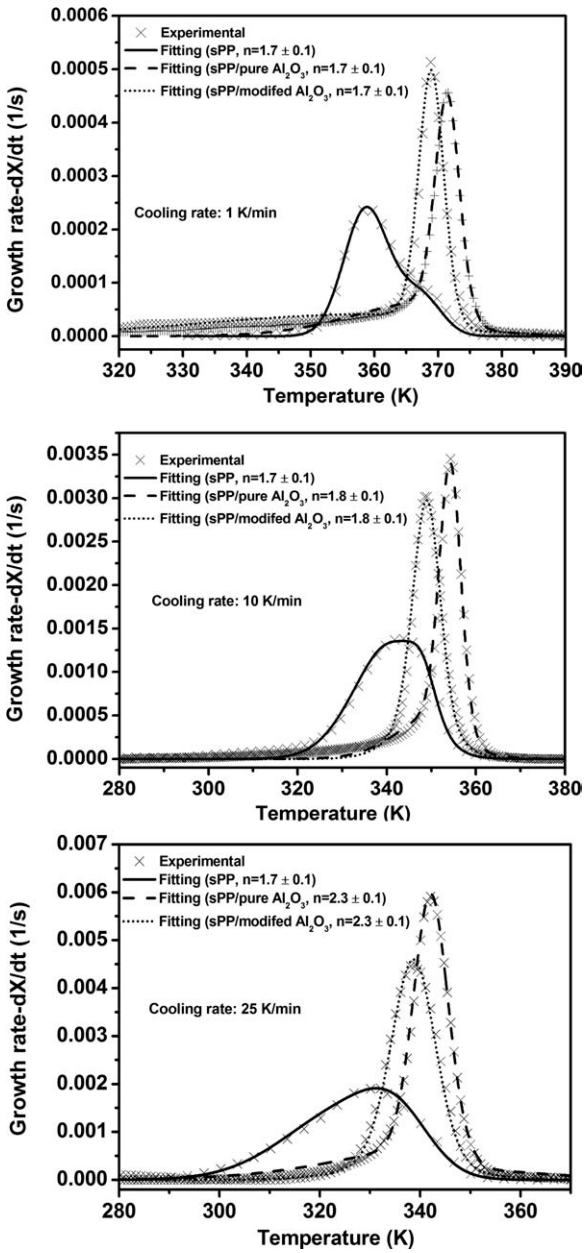

Figure 9 Crystal growth rate of sPP, sPP/pure alumina, and sPP/modified alumina. A comparison between experimental data and the fitting of the Nakamura model for nonisothermal melt crystallization.

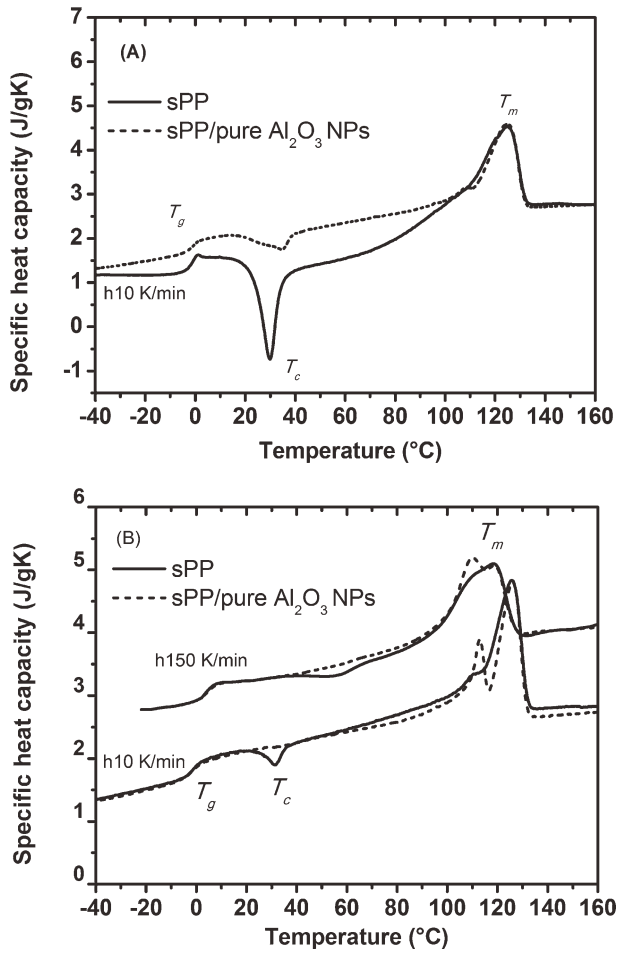

Figure 10 Subsequent melting thermograms of neat sPP and sPP/pure Al_2O_3 nanocomposites after nonisothermal melt crystallization at cooling rates of 100 K/min (A) and 25 K/min (B). Subsequent heating at 10 or 150 K/min.

there is less time for the crystal perfection and recrystallization. The sPP nanocomposites show a decrease in cold crystallization compared to pristine sPP. It is obvious that the presence of alumina nanoparticles changed both the cold crystallization and the recrystallization of sPP. The cold crystallization process is sensitive to the addition of alumina nanoparticles and crystallization conditions. The decrease in the intensity of the cold-crystallization peaks suggests that either more stable crystallites are formed or higher crystallinity is achieved for the first crystallization in the presence of nanoparticles.

CONCLUSIONS

The nonisothermal crystallization behavior of sPP and sPP/alumina nanocomposites was studied. The analysis of the nucleation process indicated that both pure Al_2O_3 nanoparticles and hydrophobically modified ones are active substrates for the heterogeneous nucleation of sPP. The modified surface reduces the nucleation activity of alumina nanoparticles in sPP/Al_2O_3 nanocomposites. Kinetic parameters obtained from the Nakamura model provided a description of the nonisothermal crystallization behavior of sPP and sPP nanocomposites. The average values of the Avrami exponent n of 1.7 indicate that a two-dimensional growth is the predominant mechanism of crystallization. The value of n did not change for neat sPP at 1, 10, or 25 K/min. For the sPP/Al_2O_3 nanocomposites at a faster cooling rate, 25 K/min, the n-values are 2.3, indicating a deviation from disk-like growth or sporadic nucleation. The incorporation of alumina nanoparticles reduces both the cold crystallization and the recrystallization of sPP during a subsequent heating run. This can be explained by the nucleating effect of the Al_2O_3 nanoparticles.

This work is part of the Petromaks project "Electrical Insulation Materials and Insulation Systems for Subsea High-Voltage Power Equipment" funded by the Research Council of Norway and the industrial partners Deutsch, Nexans Norway AS, Statoil ASA, Total E&P Norge AS and Vetco Gray-Ge Oil and Gas. Thanks are owing to Kjell Windsland for DSC contributions.

References

1. Wilkinson, A. N.; Ryan A. J. Polymer Processing and Structure Development; Kluwer Academic Publishers: The Netherlands, 1999.
2. Yoshino, K.; Ueda A.; Demura, T.; Miyashita, Y.; Kurahashi, K.; Matsuda, Y. Proceedings of the 7th International Conference on Properties and Applications of Dielectric Materials, Nagoya, 2003, 175.
3. Yoshino, K.; Demura, T.; Kawahigashi, M.; Miyashita, Y.; Kurahashi, K.; Matsuda, Y. Electrical Eng Jpn 2004, 146, 18.
4. Kurahashi, K.; Matsuda, Y.; Miyashita, Y.; Demura, T.; Ueda, A.; Yoshino, K. Electrical Eng Jpn 2006, 155, 1.
5. Rosa, C. D.; Auriemma, F. Prog Polym Sci 2006, 31, 145.
6. Supaphol, P.; Spruiell, J. E. Polymer 2001, 42, 699.
7. Supaphol, P.; Thanomkiat, P.; Phillips, R. A. Polym Test 2004, 23, 881.
8. Supaphol, P.; Spruiell, J. E. J Appl Polym Sci 2000, 75, 44.
9. Grasruck, M.; Strobl, G. Macromolecules 2003, 36, 86.
10. Schmidtke, J.; Strobl, G.; Thurn-Albrecht, T. Macromolecules 1997, 30, 5804.
11. Uehara, H.; Yamazaki, Y.; Kanamoto, T. Polymer 1996, 37, 57.
12. Pucciariello, R.; Villani, V.; Guadagno, L.; Vittoria, V. Polym Eng Sci 2006, 46, 1433.
13. Kaempfer, D.; Thomann, R.; Mulhaupt, R. Polymer 2002, 43, 2909.
14. Cerrada, M. L.; Rodriguez-Amor, V.; Perez, E. J Polym Sci: B Polym Phys 2007, 45, 1068.
15. Pucciariello, R.; Villani, V.; Guadagno, L.; Vittoria, V. Polym Eng Sci 2006, 46, 1433.
16. Chae, D. W.; Shim, K. B.; Kim, B. C. J Appl Polym Sci 2008, 109, 2942.
17. Zhao, H.; Li, R. K. Y. J Polym Sci: B: Polym Phys 2005, 43, 3652.
18. Wunderlich, B. Macromolecular Physics; Academic Press: New York, 1976.
19. Nakamura, K.; Katayama, K.; Amano, T. J Appl Polym Sci 1973, 17, 1031.

20. Nakamura, K.; Watanabe, T.; Katayama, K.; Amano, T. J Appl Polym Sci 1972, 16, 1077.
21. Nakamura, K.; Watanabe, T.; Amano, T.; Katayama, K. J Appl Polym Sci 1974, 18, 615.
22. Avrami, M. J Chem Phys 1941, 9, 177.
23. Evans, U. R. Trans Faraday Soc 1945, 41, 365.
24. Mathworks Inc., Available at: http://www.mathworks.com.
25. Glomsaker, T.; Larsen, Å.; Andreassen, E. Polym Eng Sci 2005, 45, 945.
26. Truong, L. T.; Larsen, Å.; Holme, B.; Diplas, S.; Hansen, F. K.; Roots, J.; Jørgensen, S. Surf Interface Anal 2010, 42, 1046.
27. Available at: http://rsbweb.nih.gov/ij/.
28. Lee, J. K.; Choy, J. H.; Choi, Y. Surf Sci 1991, 256, 147.
29. Truong, L. T.; Larsen, Å.; Holme, B.; Hansen, F. K.; Roots, Polymer 2011, 52, 1116.
30. Supaphol, P. J Appl Polym Sci 2000, 78, 338.
31. Supaphol, P. J Appl Polym Sci 2001, 82, 1083.